Sulfated Nanocapsular Aluminas: Controlling their Brönsted and Lewis Acidity

ARTICLE *in* THE JOURNAL OF PHYSICAL CHEMISTRY C · SEPTEMBER 2009

Impact Factor: 4.77 · DOI: 10.1021/jp905603j

Sulfated Nanocapsular Aluminas: Controlling their Brönsted and Lewis Acidity

Jaime S. Valente,*,†,‡ Esteban López-Salinas,† Xim Bokhimi,§ Jorge Flores,‡ Ana M. Maubert,‡ and Enrique Lima||

Instituto Mexicano del Petróleo, Eje Central No. 152, 07730 México D. F., México, Universidad Autonoma Metropolitana-A, Química de Materiales, Avenida San Pablo No. 180, 02200 México D. F., México, Instituto de Física, UNAM, A.P. 20-364, 01000 México D. F., México, and Instituto de Investigaciones en Materiales, UNAM, A. P. 70-360, 04510 México D.F., México

Received: June 15, 2009; Revised Manuscript Received: August 1, 2009

Sulfated aluminas were prepared by a sol−gel method, using sulfuric acid as both hydrolysis catalyst and sulfate source. The nominal amount of sulfate was varied between ~2 and 17% wt. Solids thus obtained present unique nanocapsular morphology with capsules' shells made up of Al−O polynuclear species, which crystallized into boehmite when aged for 30 days. Upon calcination, small γ-alumina crystals were obtained, which present large surface areas and pore volumes. The presence of sulfate ions generated strong Brönsted acid sites, while Lewis acid sites were present in the coordinatively unsaturated sites of tetracoordinated and pentacoordinated aluminum atoms, as was demonstrated by both pyridine adsorption followed by FTIR and ^{27}Al MAS NMR. Catalytic performance was tested using 2-propanol conversion as a model reaction, showing a marked dependence of activity and selectivity with sulfate loading.

1. Introduction

Aluminas are perhaps the transition metal oxides most widely used as catalysts and catalyst supports. They have been employed in a variety of chemical, petrochemical and petroleum refining processes.[1] Their main advantages are their low cost, good thermal stability, high specific surface area, surface Lewis acidity, and the important interaction that they exhibit with deposited transition metals.[2−4] Aluminas are generally produced industrially by precipitation, drying, and calcination of aluminum oxy-hydroxides.

The catalytic properties of aluminas largely depend on their crystalline structure and texture. Therefore, a great effort has been devoted to master these physicochemical properties.[4−10] Recently, several research groups worldwide have driven their efforts to synthesize nanostructured aluminas to control their textural properties. Hence, many strategies to obtain such characteristics have been proposed; for instance, the use of hypercritical drying conditions of xerogels[11,12] and the employment of surfactant assemblies.[13−16]

The activity and selectivity of aluminas as catalysts are also intimately related to the amount, strength, and nature of acid sites.[17−19] Additionally, control over acid sites type and population is highly desirable, as Brönsted acid sites are necessary in certain reactions to achieve skeletal rearrangements. Thus, with the idea of changing and adjusting alumina acidity, several strategies have been proposed, that is, doping it with sulfate or phosphate ions to create Brönsted acid sites.[19−22] Furthermore, the Lewis acidity is related to aluminum coordination and to the chemical nature of its neighbors. The creation of 4-fold (Al^{IV}) and 5-fold (Al^{V}) species of aluminum coordinately unsaturated sites (CUS), their amount, vicinity, and accessibility could be the key to controlling the acidity.[17] Conventionally, aluminas are dehydrated during preparation, producing CUS that are accompanied by a redistribution of the charge on the aluminum and oxygen atoms, and thus creating Lewis acidity.

In the scientific literature, it is claimed that when doping the alumina surface with sulfate ions, the overall Lewis acidity should decrease, as part of the surface is occupied by thermally stable sulfate groups and thus, a lower amount of CUS cations can be produced upon activation. The residual Lewis acidity has sometimes been observed to increase in strength due to inductive effects from the charge-withdrawing sulfate groups.[22,23]

Previously, the authors have reported the synthesis of sulfated aluminas by a simple sol−gel procedure, using different amounts of sulfuric acid as both hydrolysis catalyst and as sulfate source.[20,21] It was found that the as-prepared powders were made up of hollow spheres or capsules with diameters between 10 and 50 nm, a morphology that has not been obtained when using other synthetic procedures.[20,21]

Upon aging at room temperature for a variable number of days (up to 30), these nanocapsules were found to interact with each other and aggregate.[20] Aggregation and coalescence of the capsules were hindered when peptizing ions are present in the solvent,[24] since these anions surround the colloidal-sized nanocapsules and obstruct the capsule−capsule interaction. This peptizing effect was observed with sulfuric acid; it has been demonstrated that the interaction between the nanocapsules in the sol decreased as the sulfate ion concentration in it increased.

This interaction induces partial crystallization of the atomic local distribution in the shells from the noncrystalline state into the atomic distribution of crystalline boehmite.[20] The X-ray diffraction patterns of the aged samples with different sulfate amounts showed boehmite peaks along with the noncrystalline phase obtained in the unaged samples. XRD patterns show that boehmite concentration and crystallinity decreased when the SO_4^{2-}/Al molar ratio was increased. Thus, crystallization of the nanocapsules' shells into boehmite depended on the interaction between capsules and on sample aging, which induced atom

* To whom correspondence should be addressed. Phone: + 52 (55) 9175-8444. E-mail: jsanchez@imp.mx.
† Instituto Mexicano del Petróleo.
‡ Universidad Autonoma Metropolitana-A.
§ Instituto de Física.
|| Instituto de Investigaciones en Materiales.

10.1021/jp905603j CCC: $40.75
Published on Web 08/25/2009

reordering.[20] After annealing at 550 °C, the boehmite was pseudomorphically transformed into γ-alumina.

In the present work, a method for controlling the Brönsted and Lewis acidity over sulfated γ-aluminas obtained by calcination of these sol−gel boehmite samples is proposed. The effect of the sulfate amount, introduced as sulfuric acid during boehmite synthesis, on the type of acidity was studied, as well as the textural and catalytic properties of aluminas. The sol−gel method was used to prepare sulfated aluminas because it provides an attractive and convenient route to manipulate the structural and textural properties and purity of product.[12,19,25,26] Pyridine adsorption followed by FTIR was used to determine the type and strength of the different acid sites. Also, the acidic function properties of sulfated aluminas have been investigated in the conversion of 2-propanol, because depending on the acidic or basic nature of the solids three different reactions can occur, dehydrogenation, dehydration, and/or coupling.[27]

2. Experimental Section

2.1. Synthesis of Materials. The synthesis procedure of sulfated aluminas has been described previously.[21] Briefly, aluminum tri*sec*-butoxide (ATB) was used as aluminum source and anhydrous 2-propanol as solvent. ATB was dissolved and refluxed for 1 h. Sulfuric acid was added dropwise, and the solution was refluxed and stirred at 85 °C for 1 h. Afterward, deionized water was added. The gel was placed in a glass vessel and aged for 30 days at room temperature. Afterward, the product was dried at 120 °C. The molar ratios 2-propanol/ATB = 60 and H_2O/ATB = 1 were constant. The molar ratio H_2SO_4/ATB was 0.01, 0.03, 0.06, or 0.09, resulting in nominal 1.92, 5.77, 11.54, and 17.32% wt H_2SO_4, respectively. The samples were labeled as ASO4-0.01, ASO4-0.03, ASO4-0.06, ASO4-0.09, respectively. Dried solids were calcined at two different temperatures from room temperature up to 550 or 700 °C for 4 h at 4 °C min^{-1} heating ramp. Calcined samples were labeled ASO4-X-C*Y*, where X is the H_2SO_4/ATB molar ratio, and *Y* indicates calcination temperature (550 or 700 °C). In thermal analyses and FTIR (sulfate studies) only dried materials were used, so samples were referred to only as ASO4-X.

2.2. Experimental Techniques. ***Textural Analysis.*** Specific surface area and pore size distribution were obtained from nitrogen adsorption−desorption isotherms measured in a Micromeritics ASAP-2100 analyzer. The adsorption was carried out on calcined solids (550 °C) after outgassing at 400 °C under a 10^{-5} Torr residual pressure during 4 h. The surface areas were calculated by the Brunauer−Emmett−Teller (BET) method, and the pore size distribution and total pore volume were determined by the Barret−Joyner−Halenda (BJH) method.

Thermal Analysis. Weight loss of sulfated aluminas (dried at 120 °C) as a function of temperature was recorded in a Perkin-Elmer TGA-7 using a linear 10 °C min^{-1} heating rate and 20 cm^3 min^{-1} flow of dry air from room temperature to 1000 °C.

Infrared Spectroscopy. For pyridine adsorption measurements, IR spectra were obtained at a resolution of 4 cm^{-1} in the range of 1700−1400 cm^{-1} using a Perkin-Elmer model 170-SX FTIR spectrometer. A wafer of sample was mounted in a pyrex vacuum cell fitted with CaF_2 windows. The samples were pretreated at 550 °C for 1 h in a stream of O_2 followed by evacuation at 550 °C, then cooled to room temperature to obtain the background IR spectra. The sample was evacuated to 7.5 × 10^{-4} Torr, followed by exposure (2.14 L h^{-1}) to pyridine-saturated N_2 for 15 min, then outgassed 1 h at room temperature (pressure 7.5 × 10^{-4} Torr), and finally linearly heated up to the desire temperature.

The concentration of Brönsted and Lewis acid sites was obtained using a standard procedure based on the Lambert−Beer law.[28] The absorbency (A_I) is determined as the integrated area under the curve as follows

$$A_I = B \cdot C \cdot \int e_v d_v \quad (1)$$

Where $\int e_v\, d_v$ is the extinction coefficient and it is proportional to $0.4343 \cdot I_v$. It is generally accepted that $I_v = 3.03$ cm μmol^{-1} and 3.26 cm μmol^{-1} for the bands at 1545 and 1450 cm^{-1}, respectively.[29] *B* is related to weight /area (g cm^{-2}) wafer ratio, and *C* is the concentration of Brönsted or Lewis acid sites, which can be calculated as

$$C_{\text{Brönsted}} = \frac{A_I(1545\ \text{cm}^{-1})}{\text{weight/area} \cdot (0.4343 \cdot 3.03)}$$

$$C_{\text{Lewis}} = \frac{A_I(1450\ \text{cm}^{-1})}{\text{weight/area} \cdot (0.4343 \cdot 3.26)}$$

For the measurements concerning the sulfate vibration bands, the activation of the samples was conducted in a quartz IR cell. A wafer was heat-treated in flowing O_2 at a given temperature (100−500 °C) for 1 h, the sample was then cooled to room temperature and an FTIR spectrum was recorded, in the range of 1700−1000 cm^{-1}.

^{27}Al MAS NMR Measurements. The ^{27}Al MAS NMR spectra were acquired on a Bruker ASX 300 Spectrometer operating at resonance frequency of 78.2 MHz. ^{27}Al MAS NMR spectra were obtained after short single pulses (π/12) with a repetition time of 500 ms. The samples were spun at 10 kHz and the chemical shifts were referenced to 1 N aqueous solution of $AlCl_3$. A rough estimation of the number of (AlO_x) species was attempted by fitting Gaussian/Lorentzian lines to the peaks, calculating the area under the peaks and dividing it by the total area in order to obtain each species' percent; the Bruker software WIN NMR was used for this end. However and given the second-order quadrupolar broadening included in these peaks due to the use of conventional (<400 MHz) magnetic fields, limited use of these numbers should be acknowledged since they serve mainly to identify (AlO_x) population trends among the samples of this study.

2.3. Catalytic Tests. The 2-propanol (J.T. Baker) conversion was carried out at 130 °C and atmospheric pressure in a differential fixed bed tubular reactor. The partial pressure of the reactant was 8.3 Torr. Samples were pretreated in situ in flowing N_2 at 550 °C for 1 h. Reaction products were analyzed by online GC in a Varian CP-3800 chromatograph equipped with a FID and a Perkin-Elmer 30 m capillary column.

3. Results and Discussion

3.1. Textural Properties. The textural properties of calcined (550 °C/4 h) sulfated aluminas upon varying sulfate amounts are presented in Table 1. Nitrogen adsorption−desorption isotherms are shown in Figure 1; all isotherms are type IV according to IUPAC classification. Said isotherm characterizes mesoporous solids; however, the relative pressure (P/P_o) where the distinctive rounded knee should appear is very low. In fact, its presence is not so perceptible, pointing to the weak adsorption enthalpy between adsorbate and adsorbent, and indicating that a multilayer adsorption process takes place from the very

TABLE 1: Textural Properties of Sulfated Aluminas, Prepared with Varying H_2SO_4/ATB Molar Ratio, after 30 Days Aging at Room Temperature and Calcined at 550°C

sample	BET surface area (m^2 g^{-1})	pore volume (cm^3 g^{-1})	average pore diameter (nm) I	II
ASO4-0.01C550	386	1.82		
ASO4-0.03C550	317	0.97	9	20−60
ASO4-0.06C550	456	1.44	6	20−60
ASO4-0.09C550	435	1.62	5	35

beginning.[30] Furthermore, *t*-method micropore volume was negligible in all cases.

Pore size distribution (inset in Figure 1) is drastically modified as the amount of sulfate increases. Sample ASO4-0.01-C550 has a distribution between 3 and 100 nm with the peak centered at ∼15 nm and with a small shoulder appearing between 20 and 60 nm. Increasing sulfate amount (sample ASO4-0.03-C550) results in a wider distribution centered at ∼9 nm. The shoulder between 20 and 60 nm becomes appreciably more important and contributes to a larger proportion of the pore volume, denoting the presence of both meso- and macropores. This tendency continues when increasing the sulfate amount, until sample ASO4-0.09-C550, where the main porosity is centered at ∼35 nm with an important contribution of macropores and only a shoulder in the region between 5 and 10 nm.

The above results can be explained by considering the lower porosity to be ascribed to intraparticle porosity, while the larger pores are created by faulty particle stacking upon calcination, creating larger and more irregular pores. It has been previously observed by transmisssion electron microscropy and X-ray diffraction (XRD) that in samples with lower amounts of sulfate, the capsules coalesce and crystallize better;[20,21] therefore, there is a lower proportion of interparticle voids. On the other hand, the sample with the highest sulfate content also has the largest proportion of nonagglomerated capsules, favoring large interparticle porosity.

In Table 1, the sample with molar ratio = 0.03 has the lowest surface area, 317 m^2 g^{-1}, while sample ASO4-0.06-C550 has the largest area, 456 m^2 g^{-1}. Also, very large pore volumes were obtained from 0.97 cm^3 g^{-1} in ASO4-0.03-C550 reaching up to 1.82 cm^3 g^{-1} in the sample with lowest sulfate content.

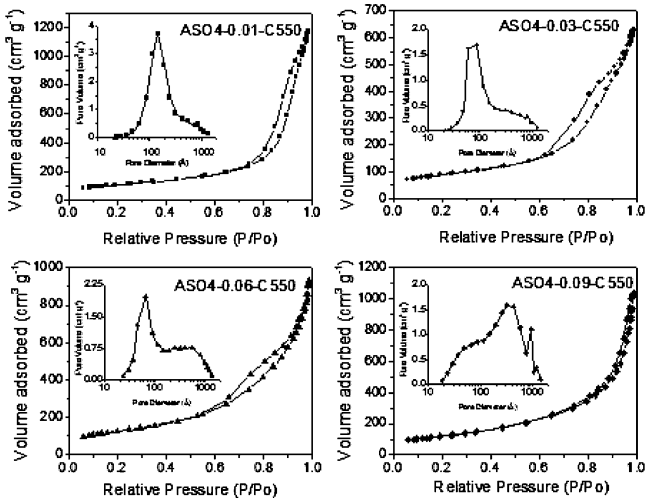

Figure 1. Nitrogen adsorption−desorption isotherms of calcined samples (550 °C/4 h) with pore size distribution displayed as an inset.

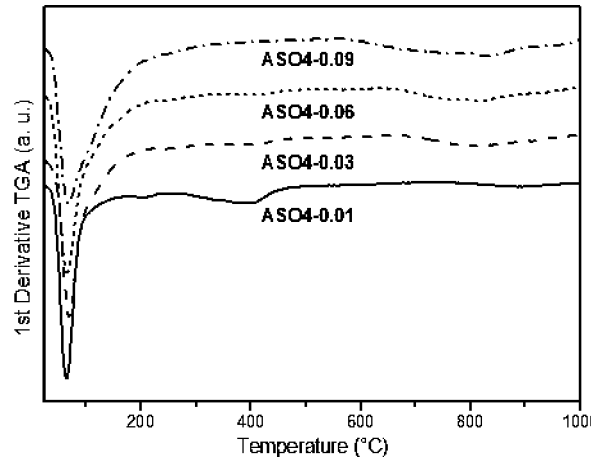

Figure 2. First-derivative of TGA profiles from sulfated sol−gel aluminas.

TABLE 2: Weight Loss Values and Temperatures of Sulfated Sol-Gel Aluminas

sample	temperature (°C)	weight loss (wt %)	total (wt %)
ASO4-0.01	63	22.78	35.73
	404	10.79	
	897	2.16	
ASO4-0.03	70	29.83	44.0
	413	8.21	
	819	5.96	
ASO4-0.06	65	32.8	47.75
	416	7.47	
	822	7.48	
ASO4-0.09	67	45.22	54.8
		7.43	
	831	9.55	

However, there appears to be no direct correlation between pore volume, surface area, and sulfate amount.

Two key points should be highlighted. On the one hand, the textural properties of the sol−gel sulfated aluminas are comparable, or even superior, to mesoporous aluminas prepared in aqueous solutions with anionic, cationic, or nonionic surfactants;[16] pore volumes above 1 cm^3 g^{-1} are not so easy to obtain. On the other hand, textural properties are not affected by sulfate loading, contrary to what is traditionally observed when sulfate groups are impregnated on a γ-alumina. For instance, when impregnating γ-alumina with ammonium sulfate, the specific surface area decreased significantly as the amount of sulfate increased (220−151 m^2 g^{-1} for 0−10% wt sulfate, respectively).[31]

3.2. Thermal Analyses. Weight loss patterns of boehmite are generally characterized by a steep drop below 200 °C and another weight loss at about 400 °C.[32] The thermogravimetric analysis profiles (first derivative) of sol−gel sulfated aluminas are shown in Figure 2. They are similar to those of common boehmites, except for the following two features, which clear out as the sulfate loading increases: (i) the weight loss at 400 °C becomes negligible and (ii) the weight loss at around 800 °C becomes considerable. Another feature that deserves attention is the widening of all peaks as sulfate loading increases, which may be associated with the relatively small crystallites that were observed previously by XRD analyses.[21]

In Table 2, the weight loss between 60 and 70 °C, associated with physisorbed water, for all sulfated alumina samples increased from 22.8 to 45.2% as the H_2SO_4/ATB ratio increased from 0.01 to 0.09, indicating a modification of alumina's surface hydrophilicity as sulfate content increases. This weight loss is related to desorption of water molecules in AlOOH−H_2O, which decreases as the crystal size increases.[33−35] For instance, ASO4-

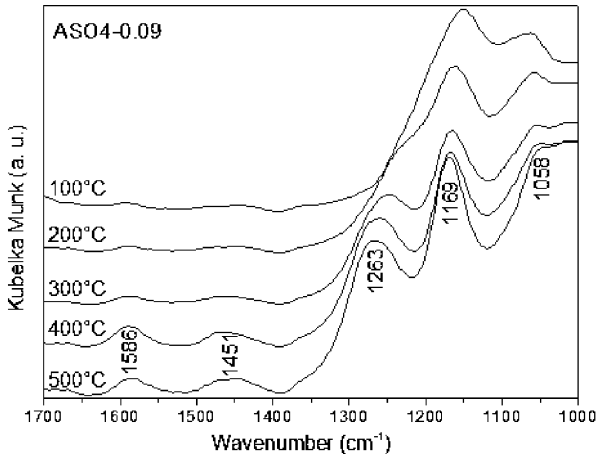

Figure 3. Temperature evolution of FTIR spectrum in the SO_3 region for sample ASO4-0.09.

0.09 showed the largest weight loss in this interval, and it is also the solid with the smallest crystal size. Furthermore, the large specific surface areas presented by all the samples entail a great water adsorption capacity.

The weight loss around 400 °C decreases as the sulfate loading rises (see Table 2). This weight loss is related to the phase transition of alumina from boehmite to γ-alumina. In agreement with XRD results,[21] higher sulfate loadings result in less crystalline boehmite phase and thus fewer phase transition weight loss.

Weight losses centered at 897, 819, 822, and 831 °C (see Table 2) from ASO4-0.01, ASO4-0.03, ASO4-0.6, and ASO4-0.09, respectively, may be ascribed to decomposition of sulfate anions, where weight loss at a lower temperature indicates a relatively weaker bond on sulfate species, while that at the highest temperature comes from a strongly attached species. Nonetheless, decomposition of weakly adsorbed sulfate species at temperatures below 800 °C is not ruled out. Comparison of weight losses around 800 °C (2.16, 5.96, 7.48, and 9.55% wt, see Table 2) with nominal H_2SO_4 wt % (1.92, 5.77, 11.54 and 17.32% wt, see Experimental Section) indicate that lower sulfate loadings result in stronger sulfate adsorption. Sample ASO4-0.09 most likely loses a significant amount of sulfate species at lower temperature.

Accordingly, Sun et al. reported the decomposition of sulfate anions between 800 and 1000 °C.[36] In sol−gel sulfated TiO_2, sulfate anions (2.2−15.5 wt %) fixed to TiO_2 surface in different modes, thermally detach from TiO_2 at temperatures between 605 and 698 °C, depending on their acid strength.[37] Similarly, Ward and Ko observed a range of sulfate species in sol−gel sulfated ZrO_2 related to different acidities.[38] Weight loss associated to sulfate anions increases from 2.16 to 9.55%, as sulfate loading increases, as indicated in Table 2. Hence, ASO4-0.09 contains more sulfate species in comparison with that of ASO4-0.01, which results in a great number of strong acid sites, as reported elsewhere.[36] Despite high sulfate loadings, it is worth mentioning that weight losses associated with sulfate multilayers and aluminum sulfate (at 630 and 800 °C, respectively), as reported elsewhere[39] for a γ-alumina impregnated with 0.2 to 4.8 M H_2SO_4, were not observed in our case.

3.4. Infrared Study. The FTIR spectra for sample ASO4-0.09 in the spectral window where SO_3 absorbs is shown in Figure 3. Only three bands were observed, even for high sulfur loadings. This suggests monodentate adsorption configuration. In fact, the relative frequencies of these peaks at 1058, 1169, and 1263 cm^{-1} are in good accord with the corresponding ν (O-SO_3) and ν_s (O-SO) and ν_a (O-SO_3) modes. Weak features were observed at 1386 and 1365 cm^{-1} in ASO4-0.06 and ASO4-0.03, respectively, which is associated with typical bidentate SO_4 species. It is important to note that the precise frequencies of surface SO_4 vibrational modes are sensitive to the degree of surface hydration, accounting for a wide variance in literature values.[40,41]

TABLE 3: Vibrational Modes of Pyridine in Aprotic, Lewis and Brönsted Sites[44]

H-bonded pyridine	coordinatively bonded pyridine	pyridinium ion
aprotic sites	Lewis sites	Brönsted sites
1440−1447 (19b)	1447−1464 (19b)	
1485−1490	1488−1503 (19a)	1485−1500 (19a)
		1535−1550 (19b)
1580−1600 (8a)	∼1580 (8b)	
	1600−1635 (8a)	
		∼1640 (8a)

Pyridine adsorption followed by FTIR is a well-known technique used to distinguish between Lewis and Brönsted acid sites.[42,43] The main pyridine vibrational modes, when it is adsorbed to aprotic, Lewis and Brönsted sites, are shown in Table 3.[44]

The IR spectrum of pyridine (Py) adsorbed on ASO4-0.01-C550 is shown in Figure 4. At 50 °C, the IR spectrum displays only five bands at $\bar{\nu}$ = 1612, 1592, 1578, 1490, and 1442 cm^{-1} contrary to ASO4-0.09-C550 (Figure 5) that displays seven bands at $\bar{\nu}$ = 1639, 1616, 1597, 1579, 1545, 1490, and 1446 cm^{-1}. The bands at $\bar{\nu}$ = 1612 and 1616 cm^{-1} in samples ASO4-0.01-C550 and ASO4-0.09-C550, respectively, are due to Py coordinatively bonded to Lewis acid sites of moderate strength (8a Py);[36] some authors[45] have assigned such sites to tetrahedral aluminum vacancies.

The band at 1597 cm^{-1} (ASO4-0.09-C550) could arise from the 8a mode of Lewis-type Py or from that of aprotic Py (see Table 3). The intensity of this band decreases dramatically between 50 and 100 °C, and it disappears at 200 °C. This behavior is an indication of a weak interaction with Py. Since Lewis site interactions with Py are known to be strong, then the band at 1597 cm^{-1} arises from a weak interaction between Py and aprotic OH groups. Similarly, the band at 1592 cm^{-1} in sample ASO4-0.01-C550 also corresponds to an aprotic OH group. The 8a mode of coordination compounds shifts to

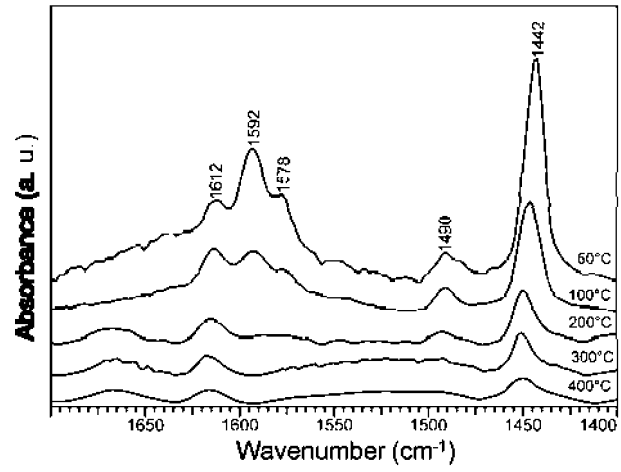

Figure 4. FTIR spectrum of pyridine adsorption on sample ASO4-0.01-C550, as a function of temperature.

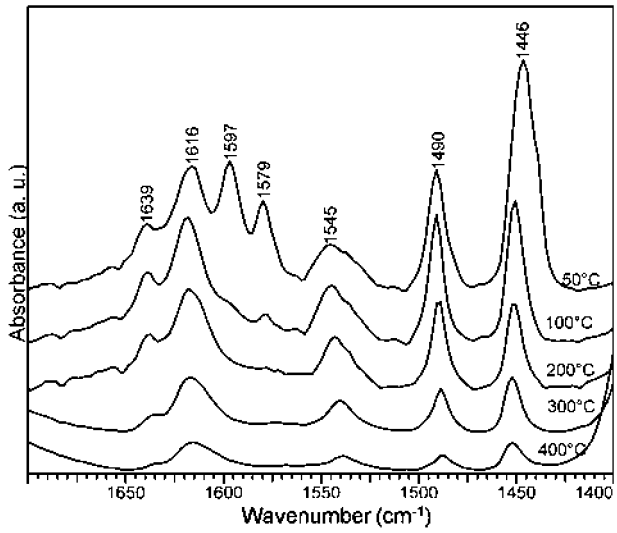

Figure 5. FTIR spectrum of pyridine adsorption on sample ASO4-0.09-C550, as a function of temperature.

increasingly higher frequencies as the coordination bond energy increases. It has also been suggested that this vibrational mode of coordinated Py would be sensitive to the coordination number of the metal center and a possible discrimination of Al^{3+} in hexa-, penta-, and/or tetracoordinated sites on alumina surfaces.[46,47]

The bands at $\nu = 1579$, 1490, and 1446 cm^{-1} are due to Py species coordinated to Lewis acid sites (8b, 19a, and 19b). In sample ASO4-0.01-C550, these bands appear at 1578, 1490, and 142 cm^{-1}. Furthermore, the bands at $\nu = 1639$ and 1545 cm^{-1} are assigned to Brönsted acid sites (8a and 19b). On sample ASO4-0.01-C550, these bands are missing, and thus Brönsted acid sites are not observed. Therefore, high loadings of sulfates lead to the appearance of Brönsted acid sites, as expected. Differences between IR-Py bands of four sulfated aluminas are most likely due to different degrees of coordinative unsaturation of Al-cations and to sulfate loadings. Also, smaller particles allow for the creation of more defects, related to the acidity of sulfated aluminas.

With temperature increase, Py is released from the surface. The amount of Py desorbed at a certain temperature depends on the adsorption strength. The Py amount that remains adsorbed on the solids at different temperatures is shown in Table 4. The results of Py adsorption clearly demonstrate that the sulfation of alumina leads to the creation of two different types of Lewis acids sites and also to the generation of Brönsted acid sites. Brönsted acidity is not detected when low sulfate loadings are used; as the sulfate amount increases, so does the strength and population of Brönsted acid sites. Besides, Py remains adsorbed on Brönsted acids sites up to 300 °C or even 400 °C in the sample with highest sulfate loading; indicating a moderate strength.

Similar results were obtained with solids calcined at 700 °C, and the Py amount retained at indicated temperatures is presented in Table 5. It is worth noting that all samples, except ASO4-0.01, present Brönsted acidity at such high annealing temperature. The sample with highest sulfate loading presents very few Brönsted acid sites, retaining Py up to 200 °C, indicating lower thermal stability of SO_4^{2-} groups, in agreement with TGA results. Sample ASO4-0.03-C700 initially has less Brönsted acid sites than ASO4-0.06-C700; however, these sites are stronger and capable of retaining Py at higher temperatures up to 400 °C. On the other hand, Lewis acid sites are stronger and more numerous on ASO4-0.06 and ASO4-0.09 after calcination at 700 °C than at 550 °C. Thus, sulfate species may be responsible for creating strong Lewis acid sites after detaching from the alumina's surface.

The presence of strong Lewis acid sites on aluminas has been related to sulfate groups, which were assumed to withdraw electrons from the metal ion thus enhancing the ability of Al^{3+} ion sites to interact directly with Py.[48] The situation here is different due to the unique nanocapsular morphology presented by these materials. Sulfate groups are located on the surface, specifically on the outer shell of the nanocapsule, and may be either occupying CUS or bridging two Al polyhedrons. The number of Lewis acid sites decreases when SO_4^{2-} groups obstruct CUS, but a stronger Lewis acid site is created when SO_4 is bridging two Al polyhedrons, due to induced charge effects.

3.5. ^{27}Al MAS NMR. The number of oxygen atoms bonded to Al atoms in aluminum oxides greatly affects the ^{27}Al NMR spectrum,[49,50] which appear, if all present, as three distinguishable peaks with maxima at ~60, ~30, and ~0 ppm, from 4-fold (AlO_4), 5-fold (AlO_5), and 6-fold (AlO_6) coordination, respectively.[51,52] Since the acidity of aluminas is related to aluminum coordination and to the chemical nature of its neighbors, the creation of (AlO_4) and (AlO_5) species, the CUS, their amount, vicinity, and accessibility are the key to controlling the acidity, and eventually the catalytic activity.[17] The ^{27}Al NMR spectra of sulfated aluminas and how they are affected by SO_4^{2-} loading and by the annealing temperature are shown in Figure 6. The materials dried at 150 °C showed spectra from almost exclusively octahedral (AlO_6) species with a maximum at ~4 ppm. At higher sulfate loadings, the population of CUS (AlO_4 and AlO_5 species) marginally increased (see Table 6). After annealing at 550 °C, the type and number of aluminum species changed markedly and the spectra were clearly made up of the three aluminum species, where (AlO_4) was between 11.6 to 17.2% and (AlO_5) from 3.5 to 11.8%, the remaining being from (AlO_6) (See Table 6). The NMR spectra at 700 °C did not vary much in comparison with those at 550 °C, pointing out the stability of the lower coordination species, on average; however, their concentration was somehow lower than that at 550 °C.

Many applications of metal oxides, such as adsorption and catalysis, depend critically on surface properties, which include Brönsted acidity or basicity, Lewis acidity, and coordination unsaturation or redox properties of the surface metal ions. Given the importance of (AlO_5) species in such applications, in our sulfated aluminas the maximum relative population of (AlO_5) was 11.8% of total Al-species and it was found in the sample that contains 17.32 wt % nominal sulfate, annealed at 550 °C. Generally, the pentacoordinated Al atoms are considered to be present in alumina's amorphous domains.[53] Accordingly, in sulfated sol−gel alumina, crystallization of boehmite is hindered by sulfate ions, resulting in larger proportion of amorphous alumina, as discussed above.

Different approaches have been taken to increase the population of pentacoordinated Al-species in transition aluminas; some procedures involve the protection of Al atoms with strongly bound organic bases, while others use the templating action of block-copolymers.[54−56] For instance, piperidine-bound to Al-(O*t*Bu)$_3$ yielded a ^{27}Al NMR spectra made up of the three differently coordinated Al-species, where considerable (not quantified) pentacoordinated Al was present; the NMR spectra, however, was taken on the amine-protected adduct and not on a heat-treated amine-depleted alumina. The use of large amounts of this toxic amine (piperidine/Al = 20) makes this procedure unattractive for industrial production.[54] In a different approach,

TABLE 4: Amount of Brönsted and Lewis Acid Sites on Samples Calcined at 550 °C/4h (μmol Py g^{-1})

	ASO4-0.01-C550		ASO4-0.03-C550		ASO4-0.06-C550		ASO4-0.09-C550	
temp (°C)	B	L	B	L	B	L	B	L
50	0	787	41	563	57	440	142	586
100	0	442	44	276	53	235	179	269
200	0	200	35	193	23	110	126	150
300	0	125	6	96	5	41	73	98
400	0	99	0	72	0	24	34	61

TABLE 5: Amount of Brönsted and Lewis Acid Sites on Samples Calcined at 700 °C/4h (μmol Py g^{-1})

	ASO4-0.01-C700		ASO4-0.03-C700		ASO4-0.06-C700		ASO4-0.09-C700	
temp (°C)	B	L	B	L	B	L	B	L
50	0	372	33	781	39	716	9	657
100	0	250	52	415	45	271	20	233
200	0	14	37	175	23	145	10	153
300	0	63	10	107	5	72	0	105
400	0	32	3	65	0	39	0	68

a sol−gel alumina obtained by specific templating with a block-copolymer (hydrogenated polyethylene-cobutylene polyethylene oxide), tuned aerosol generation and sequential thermal treatments has been claimed as being made up of 44−55% (AlO_5) species when calcined between 300−500 °C. In this work, spheroidal alumina particles (i.e., because of spray drying conditions) were made up of capsular voids that averaged 13 nm; such morphological arrangement results in very stable porous structures.[55] Similarly, the authors have reported that a sol−gel alumina with nanocapsular pores without the aid of any templating agent is able to preserve its initial morphology and yield high specific surface area and pore volume, 400 m^2 g^{-1} and 1.33 cm^3 g^{-1}, respectively, after calcining at 700 °C.[20] In a copolymer-assisted preparation of fibrous alumina, a considerable (not quantified) population of pentacoordinated Al species was formed when calcining (i.e., burning off the copolymer template) at 500 °C.[56] Recently, ultrahigh magnetic (900 MHz) field ^{27}Al MAS NMR studies have clearly demonstrated the existence of (AlO_5) species, unperturbed by quadrupolar effects located on the surface of $\gamma-Al_2O_3$, where preferential deposition of BaO on these sites lowers the intensity of the corresponding (AlO_5) signal.[57] A high magnetic field (600 MHz) MAS NMR study on $B_2O_3-Al_2O_3$ catalysts shows that 7% (AlO_5) species are formed with a B content of 3.4 wt %.[58]

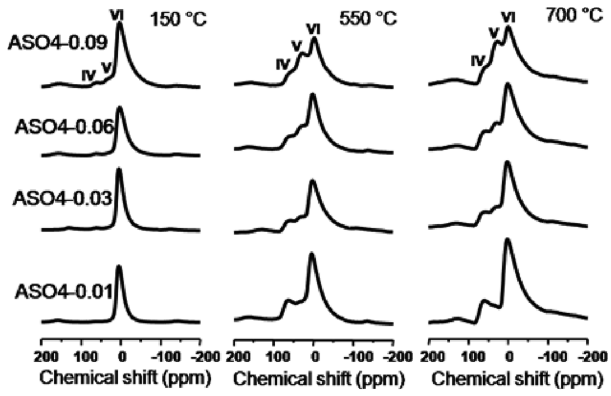

Figure 6. ^{27}Al MAS NMR spectra of samples at different calcination temperatures.

TABLE 6: Relative Population of Aluminum Species in Sulfated Sol-Gel Aluminas As a Function of SO_4^{2-} Loading and Annealing Temperature

	relative population (%)[a]		
sample	AlO_4	AlO_5	AlO_6
ASO4-0.01−150	0.0	0.0	100.0
ASO4-0.01-C550	15.6	6.9	77.5
ASO4-0.01-C700	9.7	5.8	84.6
ASO4-0.03−150	3.0	1.4	95.6
ASO4-0.03-C550	16.7	7.8	75.5
ASO4-0.03-C700	12.5	4.2	83.4
ASO4-0.06−150	2.9	1.0	96.1
ASO4-0.06-C550	15.8	8.5	76.7
ASO4-0.06-C700	13.4	4.9	81.7
ASO4-0.09−150	3.7	1.7	94.6
ASO4-0.09-C550	11.5	11.7	76.8
ASO4-0.09-C700	9.7	5.8	84.6

[a] From deconvolution and integration of spectra in Figure 6.

In typical boehmites, $(Al_4O(OH)_{10}(OH_2)_5)^0$ tetramers have been assumed as the starting building blocks.[59] Then, in sulfate-derived sol−gel boehmites it is reasonable to propose the following tetramers: $(Al_4O(OH)_{10-x}(SO_4)_{x/2}\ (OH_2)_5)^0$ or $(Al_4O(OH)_{10-x}(HSO_4)_x(OH_2)_5)^0$, where sulfate or bisulfate groups partially replace hydroxo ones. The latter groups are very likely to be present since Py adsorption-FTIR spectra (see Figures 4 and 5) indicated that the concentration of Brönsted sites is higher at higher sulfate loadings. Upon annealing, condensation of interlayer hydroxo groups of boehmite results in cross-linking of adjacent layers with concomitant collapse of the structure and formation of γ-Al_2O_3. In conventional aluminas, the initial reaction step of this crystal phase transformation is the reaction of one OH-group with the hydrogen of an adjacent hydroxo group, releasing water and forming an Al−O−Al bond. In contrast, in sulfate-mediated sol−gel alumina, OH-groups are not likely to react with sulfate anions Al−O−SO_2−O−Al because of electronic repulsion, but they may react with acid protons in bisulfate species HSO_3−O−Al.

Sulfate anions, being more difficult to thermally remove than OH-groups from metal oxyhydroxides,[60,61] play a 2-fold role. They (i) hinder nanocapsular interaction and crystallization into boehmite, and proper connection of boehmite layers to form γ-Al_2O_3 and (ii) once decomposed into gaseous SO_3 and detached from the alumina surface, create CUS, that is, 4-fold and/or 5-fold coordinated aluminum species as proposed in Scheme 2.

The Lewis acidity, as determined by Py adsorption and FTIR, is plotted as a function of percentage of CUS of aluminum and as a function of 5-fold aluminum and it is shown in Figure 7. The data plotted were chosen considering comparable experimental conditions; on the one hand, the ^{27}Al NMR spectra for ASO4-X-C550 samples and on the other the same samples after

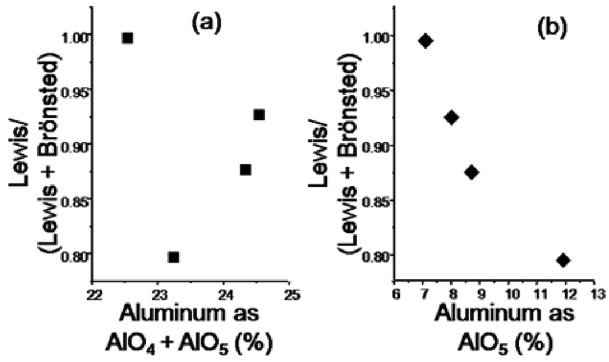

Figure 7. Lewis acidity/total acidity as a function of (a) percentage of CUS of aluminum and (b) as a function of percentage of Al^V. Data for sample series thermally treated at 550 °C previous to NMR measurements and pyridine adsorption.

SCHEME 1: Reaction Network of 2-Propanol Conversion on Acid or Basic Catalysts

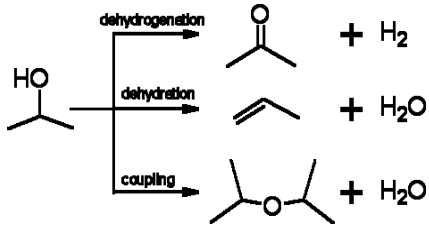

pyridine adsorption at 50 °C. There was not a clear relation between the total of CUS and Lewis acidity, but a relation was found between the percentage of 5-fold aluminum and Lewis acidity: the higher the relative Lewis acidity/total acidity, the lower the amount of 5-fold aluminum; that is, the Lewis acidity is inversely proportional to the amount of 5-fold aluminum. This trend confirms that Al^V sites can be occupied by the sulfate anions as previously proposed. Although the number of Al^V is increased with the increase of H_2SO_4/ATB, these acid sites are available to retain sulfate anions. On the contrary, the relation between CUS of aluminum ($Al^{IV} + Al^V$) fails because Al^{IV} could be partly stabilized into the framework of alumina, thus these sites are not at all available to adsorb sulfate species.

3.6. Catalytic Activity. According to literature, 2-propanol decomposes via elimination reactions that are often included in the reaction mechanisms of important industrial processes. Hydrogen and water abstraction pathways, for example, are involved in the mechanism of industrial processes such as aldol condensation of aldehydes and ketones, and lineal alcohol coupling to branched alcohols. Catalytic and mechanistic information gained using 2-propanol conversion is useful not only for characterizing surface acid−base properties but also for elucidating elimination reactions' pathway, especially on metal oxide catalysts.

2-Propanol can be converted, on several metal oxides, via three parallel reactions, dehydrogenation, dehydration, and coupling-dehydration, as shown in Scheme 1.[62] Jain and Pillai[63] demonstrated that dehydration of 2-propanol on alumina proceeds at a higher rate toward propene than toward the competitive di-isopropyl ether (DIPE) formation, even when the former reaction has a higher activation energy. This result may be explained by considering that even though secondary alcohols are more easily dehydrated than primary alcohols, ether formation from 2-propanol is not favored because it is a second-order reaction that involves the adsorption of two branched alcohol molecules on neighboring active sites offering different acid−base properties.[63,64]

SCHEME 2: Proposed Model of Sulfated Alumina and the Way Sulfate Species Detach from the Surface, Creating Coordinatively Unsaturated Sites

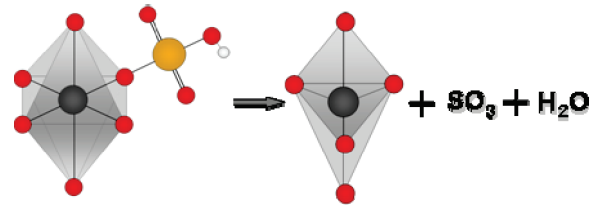

TABLE 7: Catalytic Performance of Sulfated Aluminas on the Conversion of 2-PrOH at 130 °C

catalyst	reaction rate 10^{11} (mol m^{-2} s^{-1})	selectivity (%)	
		propene	DIPE
Al_2O_3-C550	inactive		
ASO4-0.01-C550	2.6	100	0
ASO4-0.03-C550	41.0	81.2	18.7
ASO4-0.06-C550	122.8	77.3	22.6
ASO4-0.09-C550	342.5	75.5	24.5

The results of the catalytic performance of calcined (550 °C) sulfated aluminas on the conversion of 2-propanol (2-PrOH) at 130 °C are shown in Table 7 and Figure 8. In order to confirm that mass transfer does not limit the kinetics, the Thiele modulus was determined. The low values obtained (<1) guarantee that the kinetics are not perturbed by internal diffusion. The results shown in Table 7 indicate that the conversion of 2-PrOH depends on the presence of sulfates. For comparison, sample Al_2O_3−C550 with no sulfates was employed. The main products of 2-propanol conversion were propene and di-isopropyl ether (DIPE). Samples with low sulfate loadings and consequently low Brönsted acidity are little active and produce less DIPE. Activity increases with increasing sulfate loadings and DIPE production also increases. In all cases, acetone formation, which indicates the presence of basic sites, was not observed. The 2-PrOH dehydration observed on alumina has been attributed to the presence of coordinatively unsaturated sites.[41] The increase in the dehydration activity of the sulfated catalysts can be correlated to the increase of CUS upon increasing sulfate loadings and also to the increasing amount and strength of Brönsted acid sites.

According to the results shown in Table 7, DIPE formation increases as the H_2SO_4/ATB ratio rises. Some researchers claim

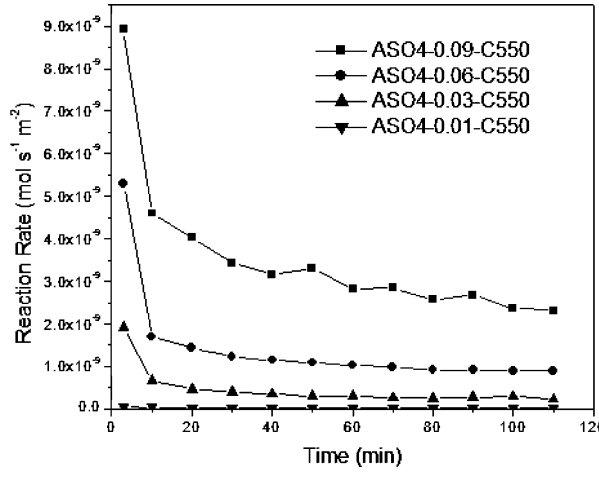

Figure 8. Catalytic activity of calcined aluminas at reaction temperature of 130 °C.

that DIPE formation depends on the oxygen vacancies or coordinatively unsaturated sites of aluminum (CUS). As was shown by ^{27}Al MAS NMR, upon increasing the H_2SO_4/ATB ratio from 0.03 to 0.09, the amount of CUS increased and thus the DIPE formation. The distribution of these aluminum species depends on the sulfate loading and calcination temperatures.

It is clear that the activity on the 2-PrOH conversion by sulfated aluminas depends on the total acidity, whereas selectivity depends on the nature and strength of acid sites. Sample ASO4-0.09-C550 showed the strongest Brönsted acid sites but also the weakest Lewis acid sites (54% of the overall Lewis acid sites were lost after annealing from 50 to 100 °C). This catalyst is highly active and less selective to propene. Therefore, based on these results, selectivity to propene is favored on strong Lewis acid sites, which are formed even when lower sulfate loadings were used, but Brönsted acid sites are necessary to improve catalytic activity. On the other hand, DIPE formation was higher on solids presenting a combination of strong Brönsted acidity and weaker Lewis acid sites.

Figure 8 indicates the typical time-on-stream behavior of sulfated aluminas during 2-propanol conversion reactions. As shown in Table 7, the sample without sulfates was inactive, whereas samples with small amounts of sulfates (ASO4-0.01-C550) produced only propene. In contrast, highly sulfated samples produced propene and di-isopropyl ether as the main products. All the catalysts deactivated during the catalytic tests; on ASO4-0.09-C550 activity decreases about 50% after 10 min on stream. The rate of formation of propene increased with increasing SO_4^{2-} content on sulfated aluminas.

2-Propanol elimination reactions on sulfated aluminas form dehydration and coupling-dehydration products via reaction pathways occurring on dual acid−base pairs that combine acid−base sites of different nature and strength. In general, dehydration of alcohols may occur through three different mechanisms, E_1, E_2, and E_{1cB}, that differ in the configuration of the transition state. On the basis of the literature, and taking into account the acid−base surface properties of the samples used in this work (mainly acids), dehydration of 2-propanol through an E_1 mechanism seems to be a correct hypothesis, since it requires catalysts containing strong Lewis acid sites.[65]

Thus, catalytic tests have shown the interrelation between structural properties and acidity of catalysts, which can be controlled from the synthesis of the boehmite precursor.

4. Conclusion

Sulfated aluminas were prepared by a sol−gel method, varying the SO_4^{2-}/ATB ratio from 0.01 to 0.09. Solids thus obtained present unique nanocapsular morphology with capsules' shells made up of Al−O polynuclear species, which crystallized into boehmite after 30 days aging at room temperature. Upon calcination, small γ-alumina crystals were obtained. Calcined solids present large surface areas and very large pore volumes. Textural properties were found not to be directly related to the sulfate amount, opposite to what is usually obtained when impregnating γ-aluminas with sulfate groups. The presence of both Lewis and Brönsted acid sites was detected by pyridine adsorption followed by FTIR. Their relative strength was determined by pyridine desorption temperature. Both acid sites are still present when annealing at temperatures as high as 700 °C. Aluminum CUS, AlO_4, and AlO_5, which are key to controlling the acidity and catalytic activity of aluminas, were identified by ^{27}Al MAS NMR. These sites may be a result of the small crystal size obtained by the sol−gel method and also by the detachment of sulfate species at high calcination temperatures. Catalytic activity was tested using 2-propanol conversion as a model reaction. The sample with the greatest sulfate loading, which contains the largest amount of Brönsted acid sites, was the most active, showing high selectivity to propene formation (dehydration path), and also formation of di-isopropyl ether. Acetone formation, which indicates the presence of basic sites, was not observed in any case. Indeed, the γ-alumina acidity can be readily controlled from the synthesis of boehmite precursor; therefore the catalytic performance shall be fine-tuned according to the intended application.

Acknowledgment. This work was financially supported by the Instituto Mexicano del Petroleo. Authors gratefully acknowledge Dr. F. Tzompantzi for performing catalytic tests and Professor J. J. Fripiat for enlightening and fruitful discussions.

References and Notes

(1) Misra, C. *Industrial Alumina Chemicals*; ACS Monograph 184; American Chemical Society, Washington, DC, 1986.
(2) Kotanigawa, T.; Yamamoto, M.; Utiyama, M.; Hattori, H.; Tanabe, K. *Appl. Catal.* **1981**, *1*, 185.
(3) Hellgardt, K.; Chadwick, D. *Ind. Eng. Chem. Res.* **1998**, *37*, 405.
(4) Knözinger, H.; Ratnasamy, P. *Cata. Rev.−Sci. Eng.* **1978**, *17*, 31.
(5) Lippens, B. C. Structure and Texture of Aluminas. Ph.D. Thesis, Uitgeverij Waltman Delft, 1961.
(6) *Preparation of Catalysts III*; Ono, T., Ohguchi, Y., Togari, O., Poncelet, G., Grange, P., Jacobs P. A., Eds.; Elsevier: New York, 1983; p 631.
(7) Trimm, D. L.; Stanislaus, A. *Appl. Catal.* **1986**, *21*, 215.
(8) Mishra, D.; Anand, S.; Panda, R. K.; Das, R. P. *Mater. Lett.* **2000**, *42*, 38.
(9) Tsuchida, T. *J. Eur. Ceram. Soc.* **2000**, *20*, 1759.
(10) Vaudry, F.; Khodabandeh, S.; Davis, M. E. *Chem. Mater.* **1996**, *8* (7), 1451.
(11) Pajonk, G. M. *Catal. Today* **1997**, *35*, 319.
(12) Schneider, M.; Baiker, A. *Catal. Rev. Sci. Eng.* **1995**, *37* (4), 515.
(13) Yada, M.; Hiyoshi, H.; Ohe, K.; Machida, M.; Kijima, T. *Inorg. Chem.* **1997**, *36*, 5565.
(14) Yang, P.; Zhao, D.; Margolese, D. I.; Chmelka, B. F.; Stucky, G. D. *Chem. Mater.* **1999**, *11*, 2813.
(15) Zhang, Z.; Pinnavaia, T. J. *J. Am. Chem. Soc.* **2002**, *124*, 12294.
(16) Handjani, S.; Blanchard, J.; Marceau, E.; Beaunier, P.; Che, M. *Microporous Mesoporous Mater.* **2008**, *116*, 14.
(17) Coster, D.; Blumenfeld, A. L.; Fripiat, J. J. *J. Phys. Chem.* **1994**, *98*, 6201.
(18) Valente, J. S.; Bokhimi, X.; Toledo, J. A. *Appl. Catal., A* **2004**, *264* (2), 175.
(19) Valente, J. S.; Falcon, S.; Lima, E.; Vera, M. A.; Bosch, P.; Lopez-Salinas, E. *Microporous Mesoporous Mater.* **2006**, *94*, 277.
(20) Bokhimi, X.; Lima, E.; Valente, J. S. *J. Phys. Chem. B* **2005**, *109*, 22222.
(21) Bokhimi, X.; Morales, A.; Valente, J. S. *J. Phys. Chem. C* **2007**, *111*, 103.
(22) Flores Moreno, J. L.; Baraket, L.; Figueras, F. *Catal. Lett.* **2001**, *77*, 113.
(23) Bolis, V.; Magnacca, G.; Cerrato, G.; Morterra, C. *Top. Catal.* **2002**, *19*, 259.
(24) Pottier, A.; Chaneac, C.; Tronc, E.; Mazerolle, L.; Jolivet, J.-P. *J. Mater. Chem.* **2001**, *11*, 1116.
(25) Livage, J. *Catal. Today* **1998**, *41*, 3.
(26) Yoldas, B. E. *J. Mater. Sci.* **1975**, *10*, 1856.
(27) Mekhemer, G. A. H.; Khalaf, H. A.; Mansour, S. A. A.; Nohman, A. K. H. *Monatsh. Chem.* **2005**, *136*, 2007.
(28) Paukshtis, E. A.; Yurchenko, E. N. *Russ. Rev.* **1983**, *52*, 3.
(29) Hughes, T. R.; White, H. M. *J. Phys. Chem. Rev.* **1967**, *71*, 7.
(30) Rouquerol, F.; Rouquerol, J.; Sing, K. *Adsorption by Powders and Porous Solids*; Academic Press: London, 1999.
(31) Kim, S. I.; Wood, S. I. *J. Catal.* **1992**, *133*, 124.
(32) Sato, T. *Thermochim. Acta* **1985**, *88*, 69.
(33) Bokhimi, X.; Sánchez Valente, J.; Pedraza, F. *J. Solid State Chem.* **2002**, *166*, 182.
(34) Guzmán Castillo, M. L.; Bokhimi, X.; Toledo, J. A.; Salmones Blásquez, J.; Hernández Beltrán, F. *J. Phys. Chem. B* **2001**, *105*, 2099.
(35) Bokhimi, X.; Toledo, J. A.; Guzmán Castillo, M. L.; Mar Mar, B.; Hernández Beltrán, F.; Navarrete, J. *J. Solid State Chem.* **2001**, *161*, 319.
(36) Sun, Y.; Yuan, L.; Ma, S.; Han, Y.; Zhao, L.; Wang, W.; Chen, C. L.; Xiao, F. S. *Appl. Catal., A* **2004**, *268*, 17.

(37) Noda, L. K.; de Almeida, R. M.; Probst, L. F. D.; Gonçalves, N. S. J. *Mol. Catal. A: Chem.* **2005**, *39*, 225.
(38) Ward, D. A.; Ko, E. I. *J. Catal.* **1994**, *18*, 150.
(39) Yang, T. S.; Chang, T. H.; Yeh, C. T. *J. Mol. Catal. A: Chem.* **1997**, *115*, 339.
(40) Bensitel, M.; Saur, O.; Lavalley, J.-C.; Morrow, B. A. *Mater. Chem. Phys.* **1988**, *19*, 147.
(41) Morterra, C.; Cerrato, G.; Bolis, V. *Catal. Today* **1993**, *17*, 505.
(42) Lercher, J. A.; Gründling, C.; Eder-Mirth, G. *Catal. Today* **1996**, *27*, 353.
(43) Busca, G. *Catal. Today* **1998**, *41*, 191.
(44) Ertl, G.; Knözinger, H.; Weitkamp, J. *Handbook of Heterogeneous Catalysts*; Wiley-VCH: New York, 1997; Vol. 2, p 710.
(45) Morterra, C.; Coluccia, S.; Chiorino, A.; Boccuzzi, F. *J. Catal.* **1978**, *54*, 348.
(46) Morterra, C.; Chiorino, A.; Ghiotti, G.; Garrone, E. *J. Chem. Soc., Faraday Trans. 1* **1979**, *75*, 271.
(47) Morterra, C.; Cerrato, G. *Langmuir* **1990**, *6*, 1810.
(48) Waqif, M.; Baachelier, J.; Saur, J.; Lavalley, J.-C. *J. Mol. Catal.* **1989**, *51*, 209.
(49) O'Reilly, D. E. *Adv. Catal.* **1960**, *12*, 31.
(50) Engelhardt, G. Introduction to Zeolite Science and Practice; Van Bekkum, H., Flanigen, E. M., Jansen, J. C., Eds.; In *Studies in Surface Science and Catalysis 58*; Chapter 8, p 285.
(51) Lippmaa, E.; Magi, M.; Samoson, A.; Engelhardt, G.; Grimmer, A. *J. Am. Chem. Soc.* **1980**, *102*, 4889.
(52) Stebbins, J. F. Nuclear magnetic resonance spectroscopy of silicates and oxides in geochemistry and geophysics. In *Handbook of Physical Constants*; Ahrens, T. J., Ed.; American Geophysical Union: Washington, DC, 1995; Vol. 2.
(53) Bagshaw, S. A.; Pinnavaia, T. J. *Angew. Chem., Int. Ed.* **1996**, *35*, 1102.
(54) Kozlov, A. I.; Kung, M. C.; Xue, W. M.; Kung, H. H. *Angew. Chem., Int. Ed.* **2003**, *42*, 2415.
(55) Boissière, C.; Nicole, L.; Gervais, C.; Babonneau, F.; Antonietti, M.; Amenitsch, H.; Sanchez, C.; Grosso, D. *Chem. Mater.* **2006**, *18*, 5238.
(56) Bai, P.; Su, F.; Wu, P.; Wang, L.; Lee, F. Y.; Lv, L.; Yan, Z.-F.; Zhao, X. S. *Langmuir* **2007**, *23*, 4599.
(57) Kwak, J. H.; Hu, J. Z.; Kim, D. H.; Szanyi, J.; Peden, C. H. F. *J. Catal.* **2007**, *251*, 189.
(58) Hansen, M. R.; Jakobsen, H. J.; Skibsted, J. *J. Phys. Chem. C* **2008**, *112*, 7210.
(59) Jolivet, J. P. *Metal Oxide Chemistry and Synthesis. From Solutions to Solid State*; J. Wiley and Sons: Chichester, 2000, p 321.
(60) Fitzgerald, J. J.; Piedra, G.; Dec, S. F.; Seger, M.; Marciel, G. E. *J. Am. Chem. Soc.* **1997**, *119*, 7832.
(61) Sun, Y.; Yuan, L.; Ma, S.; Han, Y.; Zhao, L.; Wang, W.; Chen, C.-L.; Xiao, F.-S. *Appl. Catal., A* **2004**, *17*, 268.
(62) Knozinger, H.; Khone, R. *J. Catal.* **1996**, *5*, 264.
(63) Jain, J. R.; Pillai, C. N. *J. Catal.* **1967**, *9*, 322.
(64) Di Cosimo, J. I.; Diez, V. K.; Xu, M.; Iglesia, E.; Apesteguía, C. R. *J. Catal.* **1998**, *178*, 499.
(65) Noller, H.; Kladnig, W. *Catal. Rev. Sci. Eng.* **1976**, *13*, 149.

JP905603J